



# Computational design of novel fullerene analogues as potential HIV-1 PR inhibitors: Analysis of the binding interactions between fullerene inhibitors and HIV-1 PR residues using 3D QSAR, molecular docking and molecular dynamics simulations

Serdar Durdagi<sup>a,b,\*</sup>, Thomas Mavromoustakos<sup>a,c</sup>, Nikos Chronakis<sup>d</sup>, Manthos G. Papadopoulos<sup>a,\*</sup>

<sup>a</sup>Institute of Organic and Pharmaceutical Chemistry, The National Hellenic Research Foundation, 48 Vas. Constantinou Avenue, 11635 Athens, Greece

<sup>b</sup>Department of Biology Chemistry and Pharmacy, Freie Universität Berlin, Takustr. 3, 14195 Berlin, Germany

<sup>c</sup>Department of Chemistry, University of Athens, 15784 Athens, Greece

<sup>d</sup>Department of Chemistry, University of Cyprus, PO Box 20537, 1678 Nicosia, Cyprus

## ARTICLE INFO

### Article history:

Received 3 April 2008

Revised 8 October 2008

Accepted 12 October 2008

Available online 22 October 2008

### Keywords:

HIV-1 PR

Fullerene derivatives

3D QSAR

CoMSIA

Molecular docking

Molecular dynamics simulations

LeapFrog de novo drug design

## ABSTRACT

A series of experimentally reported as well as computationally designed monoadducts and bisadducts of [60]fullerene analogues have been used in order to analyze the binding interactions between fullerene based inhibitors and HIV-1 PR employing docking studies. MD simulations of ligand-free and the inhibitor bound HIV-1 PR systems complemented the above studies and provided proper input structure of HIV-1 PR in docking simulations. The obtained results revealed a different orientation of the  $\beta$ -hairpin flaps at these two systems. In inhibitor bound system, the flaps of the enzyme are pulled in toward the bottom of the active site (the closed form) while, in ligand-free system flaps shifted away from the dual Asp25 catalytic site and this system adopts a semi-open form. The structural analysis of these systems at catalytic and flexible flap regions of the HIV-1 PR through the simulation, assisted in understanding the structural preferences of these regions, as well as, the adopted orientations of fullerene derivatives within the active site of the enzyme. Five different combinations of stereoelectronic fields of 3D QSAR/CoMSIA models were obtained from the set of biologically evaluated and computationally designed fullerene derivatives (training set = 43, test set = 6) in order to predict novel compounds with improved inhibition effect. The best 3D QSAR/CoMSIA model yielded a cross validated  $r^2$  value of 0.739 and a non-cross validated  $r^2$  value of 0.993. The derived model indicated the importance of steric (42.6%), electrostatic (12.7%), H-bond donor (16.7%) and H-bond acceptor (28.0%) contributions. The derived contour plots together with de novo drug design were then used as pilot models for proposing the novel analogues with enhanced binding affinities. Such structures may trigger the interest of medicinal chemists for novel HIV-1 PR inhibitors possessing higher bioactivity.

© 2008 Elsevier Ltd. All rights reserved.

## 1. Introduction

In the last few years, many potent human immunodeficiency virus type I aspartic protease (HIV-1 PR) inhibitors have been developed and approved as drugs for the inactivation of this enzyme by the Food and Drug Administration, while several others are under clinical investigation.<sup>1,2</sup> Since the nature of most of these drugs is peptide-like, their oral bioavailability and half-life are limited.<sup>3</sup> Experimental findings indicate the rapid emergence of drug resistance to most of the HIV-1 PR inhibitors, because site specific mutations in the enzyme occur at one or more

residues,<sup>4</sup> and references there in. These mutations are conservative and involve a similar set of amino acid residues in response to exposure to different inhibitors, thus giving rise to cross resistance.<sup>4</sup> Therefore, several research groups tried to develop non-peptidic HIV-1 PR inhibitors, which may block the mutations responsible for this resistance.<sup>4,5</sup>

The active site of the HIV-1 PR is approximately an open-ended cylindrical hydrophobic cavity with 10 Å diameter composed of catalytic aspartic acid residues Asp25 and Asp25'.<sup>6</sup> The complementary spatial relationship between [60]fullerene and the active site of the HIV-1 PR enzyme has led to the suggestion that fullerene-based derivatives might have potential use as effective HIV-1 PR inhibitors.<sup>6,7</sup> The binding interactions of [60]fullerene derivatives in the active site of the HIV-1 PR have been examined through a combination of several molecular modeling techniques.<sup>5,8</sup> Kinetic

\* Corresponding authors. Tel.: +30 2107273894 (S.D.).

E-mail addresses: [durdagis@eie.gr](mailto:durdagis@eie.gr) (S. Durdagi), [mpapad@eie.gr](mailto:mpapad@eie.gr) (M.G. Papadopoulos).

analysis of the HIV-1 PR enzyme in the presence of various water-soluble fullerenes show a competitive mode of action.<sup>5,8</sup> This is referred to the ability of fullerene derivatives to form bonds between its pendant groups and catalytic site of the enzyme as well as the van der Waals interactions with the non-polar HIV-1 PR binding site surface, thus improving the binding.<sup>5</sup>

Hitherto, a lot of fullerene derivatives have been synthesized by several experimental groups but a limited number of them have been subjected to bioactivity test against HIV-1 PR. Recently, a stable quantitative structure–activity relationships (QSAR) model has been reported by our group<sup>9</sup> using these biologically evaluated synthetic fullerene analogues.<sup>8,10–13</sup> Obviously, when the number of compounds increases in the dataset, the stability of the constructed model and the output from the model is expected to be increased. However, in this particular case, it is difficult to increase the number of compounds in the data set because the experimentally examined fullerene compounds for HIV-1 PR inhibition are limited and measured ones not show very diverse binding affinities. For this reason, an attempt has been performed for the first time to date, to our knowledge in QSAR studies: The binding energy results of biologically evaluated fullerenes in HIV-1 PR cavity was examined with Molecular Dynamics (MD) assisted docking simulations and a correlation between experimental versus theoretical values has been found. Thus, it is proposed to enlarge the data set including the structures from computationally designed compounds and their activities from the docking simulations to construct QSAR models. This idea may be used by other research groups if the experimental data are limited, binding affinities are not diverse, the coordinate file of the receptor (using X-ray data or homology model) is available and the active site of the receptor is well defined.

The large variations in binding affinities of the designed fullerene inhibitors with HIV-1 PR and the relations between biological activity and the flap motion of the enzyme, as well as, the connection between the biological activity and the conformational changes in the catalytic site of the HIV-1 PR, are discussed. The following three steps in our computational design strategy have been studied: (i) Several monoadducts and bisadducts of [60]fullerene have been designed with some modifications of reported structures in the literature (Table 1) in order to explore more conformational space. Most of the designed fullerene structures include 1,3-cyclohexadiene derivatives. The experimental methodology to synthesize this family of fullerene derivatives was reported by An et al.<sup>14</sup> (ii) In order to construct three-dimensional QSAR (3D QSAR) comparative molecular similarity indices analysis (CoMSIA)<sup>15</sup> models, both experimentally reported (Table 1) and computationally designed fullerene analogues (Table 2) and their activities (measured and calculated binding affinities) have been used. Novel monoadducts and bisadducts of [60]fullerene have been designed with the aid of 3D QSAR/CoMSIA models and their binding affinities at the HIV-1 PR have been tested employing molecular docking. In order to use proper input coordinates of [HIV-1 PR/fullerene derivative] complex in the docking simulations and to understand the reason for the large variations in the binding affinities of the designed fullerene inhibitors with HIV-1 PR, MD simulations were employed for the ligand-free and the inhibitor bound HIV-1 PR systems. Furthermore, MD simulations provided data for the analysis of the structural changes in the flap and catalytic parts of the enzyme, the connection between the biological activity and structural changes of the flap tips and the binding site of the enzyme. The flexibility of flap region of HIV-1 PR has been discussed by both experimental and computational studies.<sup>16,17</sup> The free protease adopts closed, semi-open or fully open forms in a dynamic equilibrium. However, the closed form is favored when the inhibitor is bound in the cavity of the reaction site.<sup>16</sup> Friedman et al.<sup>7,8</sup> proposed that there is a direct correlation between inhibi-

tory of a compound and the amount of hydrophobic surface area that it can desolvate. The MD simulations by Zhu et al.<sup>18</sup> showed the exclusion of water near the flap regions in order to accommodate the fullerene inhibitor. The decreasing of the water density in the cavity leads to the enhancement of the hydrophobic interaction between the fullerene derivative and the active site of the enzyme. (iii) The Leapfrog de novo drug design program<sup>19</sup> and 3D QSAR/CoMSIA contour maps have been used in order to generate a series of potent fullerene based HIV-1 PR inhibitors. This approach is fruitful and can be of general use because: (a) it minimizes the compounds to be synthesized; (b) it leads a rational design for the subsequent compounds to be synthesized and (c) it saves the time and reduces the cost and human effort.

## 2. Computational methods

### 2.1. Molecular modeling

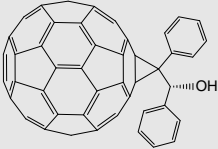
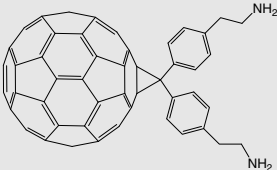
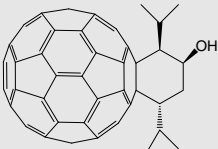
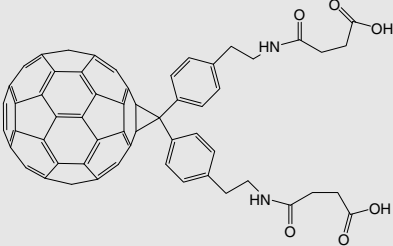
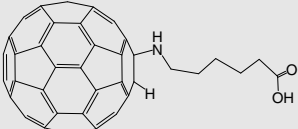
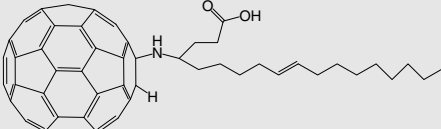
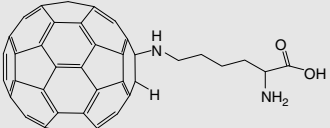
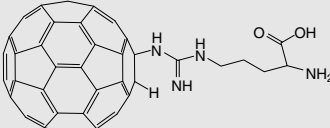
The structures of the studied fullerene molecules were subjected to full geometry optimization using the standard Tripos molecular mechanic force field of the SYBYL molecular modeling package<sup>19</sup> (Powell energy minimization algorithm<sup>20</sup>, Gasteiger–Hückel charges<sup>21</sup> and 0.001 kcal/mol Å energy gradient convergence criterions).

### 2.2. Molecular docking

Since the X-ray structure of the HIV-1 PR complexed with fullerene based inhibitors has not yet been reported, the initial structure was taken from the HIV-1 PR complexed with haloperidol derivative at 2.2 Å resolution (pdb code; 1AID).<sup>22</sup> The water molecules and the inhibitor were removed and hydrogens were added to the system. Ionization states for ionizable amino acid residues were determined according to their standard pK<sub>a</sub> values. The geometry of the enzyme has been optimized by using the Tripos molecular mechanic force field of the SYBYL molecular modeling package.<sup>19</sup> The effect of ionization states of docked compounds to the binding scores have been discussed in the literature.<sup>23–27</sup> Since ionization states of docked compounds have not yet been determined experimentally, during docking, the neutral and ionized states (aliphatic amine and carboxylic acid groups of compounds to be docked were protonated and deprotonated, respectively) were considered and compared, separately. The results related with the neutral and ionized molecules did not affect significantly the constructed 3D QSAR models, thus the neutral states of compounds were used for further analysis. Before docking, conformational analysis was applied to the ligands using the MULTI SEARCH option of SYBYL molecular modeling package.<sup>19</sup> This option locates the various energy minima available to a set of molecules, stored in a database by randomly perturbing torsions, minimizing, and eliminating duplicates. The rotatable bonds were selected for perturbed torsions using the MMP2 minimizer in SYBYL with energy convergence of 0.01 kcal/mol. The maximum number of conformers for each molecule was set to 30 and the top 10 lowest energy conformers were used in docking simulations and only the best docked complex was considered for further analysis.

Docking studies have been performed using the FlexX program of SYBYL molecular modeling package.<sup>19</sup> Since the docking scores are affected by the conformations of active site residues of the receptor, the best potent reported fullerene **1** in Table 1 has been docked at the binding site of the enzyme and the docked complex with the best binding score has been used as input in the MD simulations. The average coordinate file of HIV-1 PR from the final 1 ns trajectory files of MD simulations of complex system has been used in the redocking calculations for the compounds shown in Tables 1 and 2. It is sensible to use the conformation of HIV-1 PR obtained

**Table 1**  
Experimental and computed binding energies of reported fullerene derivatives with the HIV-1 PR.<sup>8–13</sup>

Compound No.	Compound	Experimental binding energy (kJ/mol)	Calculated binding energy (kJ/mol)	Experimental binding affinity ( $\mu\text{M}$ )
1		-40.1	-35.2	0.1
2		-30.4	-29.1	5.0
3		-39.2	-29.2	0.15
4		-29.5	-31.5	7.3
5		-36.2	-35.6	0.49
6		-16.6	-24.8	1300
7		-23.7	-32.3	75
8		-20.9	-28.1	230

(continued on next page)

Table 1 (continued)

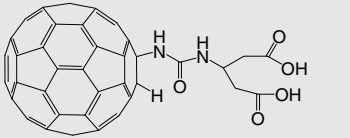
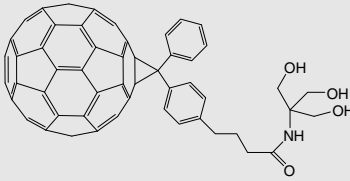
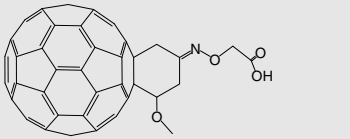
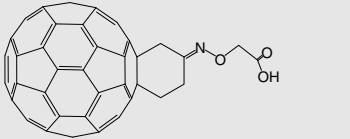
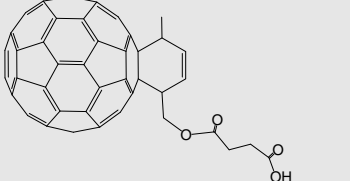
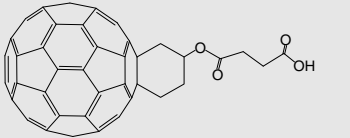
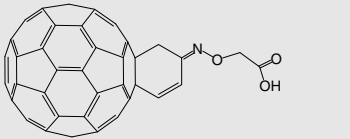
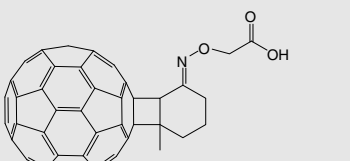
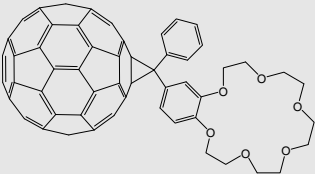
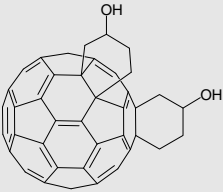
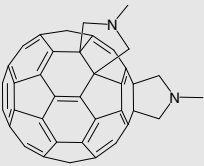
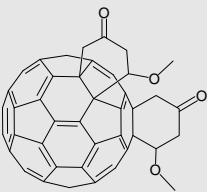
Compound No.	Compound	Experimental binding energy (kJ/mol)	Calculated binding energy (kJ/mol)	Experimental binding affinity ( $\mu\text{M}$ )
9		-22.1	-20.1	140
10		-32.2	-27.4	2.50
11		-34.7	-36.0	0.9
12		-31.8	-33.0	7.3
13		-32.5	-33.5	2.2
14		-29.9	-31.4	6.3
15		-29.5	-32.9	2.9
16		-26.8	-27.1	21.7

Table 1 (continued)

Compound No.	Compound	Experimental binding energy (kJ/mol)	Calculated binding energy (kJ/mol)	Experimental binding affinity ( $\mu\text{M}$ )
17		-22.2	-26.8	137
18		-27.3	-29.3	17.6
19		-23.8	-24.6	72.7
20		-29.4	-18.4	7.70

from MD, as input protein coordinate in the docking calculations, because the FlexX docking algorithm allows flexibility in the ligands, however it keeps the receptor rigid. The default FlexX scoring function was used for the simulations. FlexX uses formal charges, which were turned on during the docking. The active site in the docking runs, included all atoms within a radius of 6.5 Å around the critical amino acids: Asp25, Asp25', Ile50, and Ile50' (residues 25 and 50 on chains  $\alpha$  and  $\beta$ ; full list of residues of the active site has been given in the [supporting information](#)). In FlexX, an empirically derived scoring function is used to predict the binding energy. The physicochemical model behind FlexX can be divided into three parts: the analysis of the conformational space of the ligand, the model of protein-ligand interactions, and the scoring function. The scoring function of FlexX, developed by Böhm in order to rank the solutions, is an estimation of the free binding energy  $\Delta G$  of the protein-ligand complex.<sup>28</sup>

### 2.3. MD simulations

The MD simulations were performed with GROMACS 3.3.1 software package<sup>29</sup>, employing the gmx force field.<sup>30</sup> Canonical NVT ensemble at 300 K was used with periodic boundary conditions, and the temperature was kept constant by the Berendsen thermostat.<sup>31</sup> Electrostatic interactions were calculated using the particle mesh Ewald method.<sup>32</sup> Cut-off distances for the calculation of Coulomb and van der Waals interactions were 1.0 and 1.4 nm, respectively. Prior to the dynamics simulation, energy of the full system has been optimized without constraints using the steepest descent

integrator for 5000 steps. The system was then equilibrated via a 100 ps MD simulations at 300 K. Finally, a 2 ns simulation was performed with a time step of 2 fs.

### 2.4. Binding affinities

The binding affinities ( $K_i$ ) were assessed by a quantitative assay, based on the estimated binding energies of fullerene analogues with HIV-1 PR which have been determined by employing the FlexX molecular docking algorithm of Sybyl molecular modeling package. The formula  $\Delta G = -RT \ln K_i$  was used to convert the FlexX binding energies to estimated binding affinities. Since the experimental binding activities of most of the derivatives, used in this study are only reported as median effective concentration ( $EC_{50}$ ), these values are assumed to be equal with  $K_i$  in the calculations of the free binding energies. A similar working hypothesis has been used by Naik et al.<sup>33</sup> and Conn et al.<sup>34</sup> For example, the reported  $K_i$  and  $EC_{50}$  values for compound **4** are 5.3  $\mu\text{M}$  and 7.3  $\mu\text{M}$ , respectively. Assuming that  $K_i$  and  $EC_{50}$  are identical, the resulting error for  $\Delta G$  of compound **4** is 2.6 %. The logarithmic values of  $1/EC_{50}$  ( $pEC_{50}$ ) were used in the 3D QSAR correlations, as they are related to changes in the free energy of binding.

### 2.5. 3D QSAR/CoMSIA settings

Forty-three fullerene derivatives have been used in the training set to construct 3D QSAR CoMSIA models. The CoMSIA was used instead of the comparative molecular field analysis (CoMFA)<sup>35</sup>,

**Table 2**  
Computationally designed fullerene derivatives, their binding energies and estimated binding affinities.

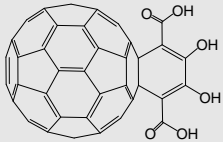
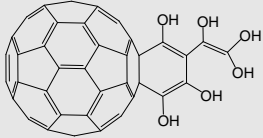
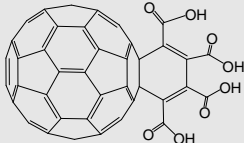
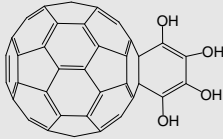
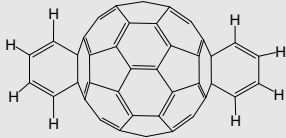
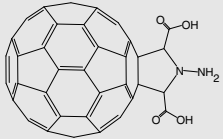
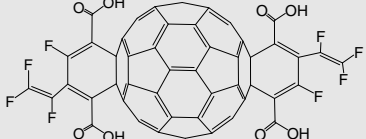
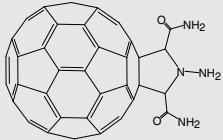
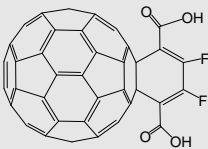
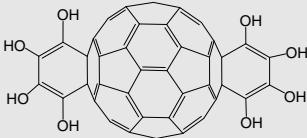
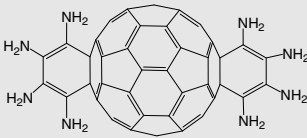
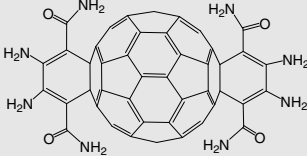
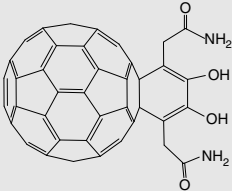
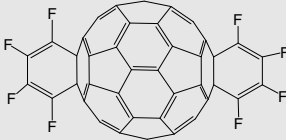
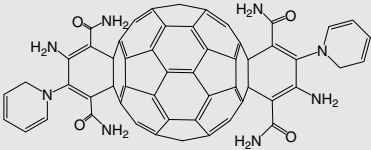
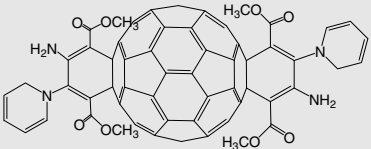
Compound No.	Compound	Calculated binding energy (kJ/mol)	Estimated binding affinity ( $\mu\text{M}$ )
21		-37.9	0.25
22		-41.9	0.051
23		-50.3	0.002
24		-35.3	0.71
25		-19.1	472
26		-35.6	0.63
27		-33.4	1.53
28		-35.5	0.66

Table 2 (continued)

Compound No.	Compound	Calculated binding energy (kJ/mol)	Estimated binding affinity ( $\mu\text{M}$ )
29		-38.4	0.21
30		-27.0	19.9
31		-27.4	16.9
32		-31.6	3.15
33		-37.6	0.28
34		-23.2	91
35		-24.3	58.7
36		-12.9	5670

(continued on next page)

Table 2 (continued)

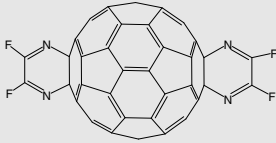
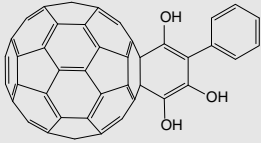
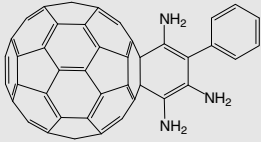
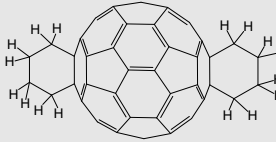
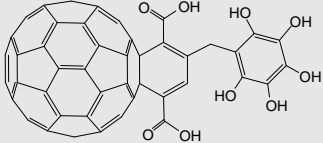
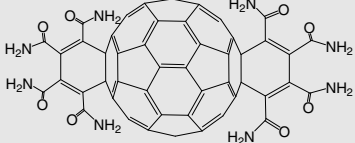
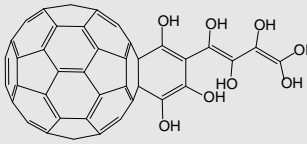
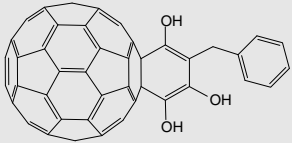
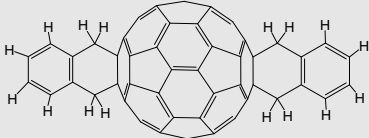
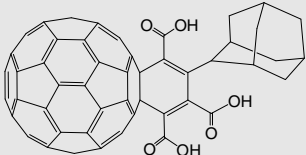
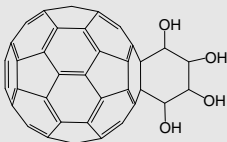
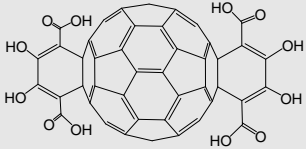
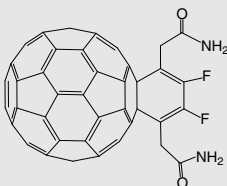
Compound No.	Compound	Calculated binding energy (kJ/mol)	Estimated binding affinity ( $\mu\text{M}$ )
37		-19.3	436
38		-32.9	1.87
39		-26.5	24.3
40		-17.6	862
41		-42.7	0.04
42		-42.6	0.04
43		-38.8	0.18
44		-32.2	2.47

Table 2 (continued)

Compound No.	Compound	Calculated binding energy (kJ/mol)	Estimated binding affinity ( $\mu\text{M}$ )
45		-23.7	75
46		-40.2	0.10
47		-35.3	0.71
48		-30.0	5.98
49		-34.9	0.84

because the energy functions typically used to calculate the field values in CoMFA can lead to significant variation of energy with very small changes in position. In CoMSIA, these fields are replaced by similarity values at the various grid positions. The similarities are calculated using much smoother potentials, which are not as steep as the Lennard–Jones and Coulombic functions and have a finite value even at the atomic positions. The use of these similarity indices is considered to lead to superior contour maps that are much easier to interpret.<sup>36,37</sup>

The steric and electrostatic field energies were calculated using the Lennard–Jones and the Coulomb potentials, respectively with a  $1/r$  distance-dependent dielectric constant in all intersections of a regularly spaced (0.2 nm) grid. A  $\text{sp}^3$  carbon atom with a radius of 1.53 Å and a charge of +1.0 was used as a probe to calculate the steric and electrostatic energies between the probe and the molecules using the Tripos force field. The truncation for both the steric and electrostatic energies was set to 30 kcal/mol. The similarity indices between the compounds and the probe atom are calculated according to:

$$A_{F,k}^q(j) = - \sum_{i=1}^n W_{probe,k} W_{ik} e^{-\alpha r_{iq}^2}$$

where  $A$  is the similarity index at the grid point  $q$ , summed over all atoms  $i$  of the molecule  $j$  under investigation;  $W_{probe,k}$  is the probe atom;  $w_{ik}$  is the actual value of the physicochemical property  $k$  of atom  $i$ ;  $r_{iq}$  is the mutual distance between the probe atom at grid point  $q$  and atom  $i$  of the test molecule;  $\alpha$  is the attenuation factor. The default value of attenuation factor  $\alpha$  was set to 0.3.<sup>37</sup> Larger values of  $\alpha$  would result in a steeper Gaussian function, increasing the attenuation of the distance-dependent effects of molecular similarity. On the other hand, reducing the value of  $\alpha$  would lead to a wider Gaussian function. The optimal value of  $\alpha$  is between 0.2 and 0.4.<sup>37</sup>

## 2.6. Partial least-squares (PLS) analysis and validations

The initial PLS analysis was performed using the “leave-one-out” cross-validation method for the 3D QSAR analysis. A minimum column filtering value of 2.00 kcal/mol was set to improve the signal-to-noise ratio by omitting those grid points whose energy variation was below this threshold. In CoMSIA analysis, descriptors were treated as independent variables whereas the  $\text{pEC}_{50}$  values were treated as dependent variables in the PLS regression analyses to derive the 3D QSAR models. The final model (non-cross-validated conventional analysis) was developed from the

model with the highest cross-validated  $r^2(r_{cv}^2)$ . The non-cross-validated models were assessed by the conventional correlation coefficient  $r^2$ , standard error of prediction, and  $F$  values.

### 2.7. Proposing compounds using cavity generation by Leapfrog

Leapfrog is a second-generation de novo drug discovery program for the design of potentially active compounds, using molecular evolution or electronic screening, by repeatedly making structural changes and then either keeping or discarding the obtained results, depending on the binding energy results.<sup>9,38–40</sup> Binding energy calculations in Leapfrog were performed by steric, electrosteric and hydrogen bonding enthalpies of ligand-cavity binding using the Tripos force field under Sybyl molecular modeling package (v. 6.8).<sup>19</sup> The cavity option was used to generate site points. The charge of the site point probe atom is positive, negative or lipophilic and its value is compared with  $\pm 1.0$ : If the value is smaller than +1.0, it is lipophilic, if the value is bigger than +1.0, site points seek a negative atom and if the value is less than  $-1.0$ , site points seek a positive atom in the approaching the fragment. Molecules **1**, **3**, **23** and **42** (monoadduct and bisadduct of [60]fullerene derivatives that have higher affinity with HIV-1 PR, Tables 1 and 2) were used as starting structures. Firstly, the OPTIMIZE module was used for the improvement of their binding energy. Secondly, JOIN, FUSE, WEED, CROSSOVER and OPTIMIZE options were performed after the initial run of 100 moves taking into consideration the synthetic difficulties. The derived ligands that had the best binding energy were used for the repeating cycle of 5000 moves.

### 3. Results and discussion

The inhibition effect of limited monoadducts and bisadducts of [60]fullerene has been biologically evaluated. Table 1 shows the biological activities of twenty fullerene derivatives reported in the literature.<sup>8,10–13</sup> In order to explore more conformational space and include more diverse binding affinities in the data set, computationally designed fullerene analogues have been analyzed using

docking and 3D QSAR studies. Both biologically evaluated and novel designed fullerene derivatives (Tables 1 and 2) have been used in the construction of 3D QSAR/CoMSIA models. A deeper understanding of the mechanistic events associated with HIV-1 PR binding is important for the design of new inhibitors with enhanced activity. Therefore, MD simulations were performed with GRO-MACS program. MD studies also help to use proper input protein coordinate in docking studies, due to the fact that the FlexX docking algorithm considers docking to a rigid protein. It is well known that, the conformations of binding pocket residues of a protein affect the binding score. The coordinates of active site residues of fullerene bound HIV-1 PR may be different than the coordinate of haloperidol derivative bound HIV-1 PR (1AID, pdb code). Hence, the correct binding mode of the studied inhibitors can best be obtained from the MD simulations of [HIV-1 PR/fullerene derivative] complex. For this reason, two different systems are used in our MD simulations: First, a fullerene-free rectangular box with HIV-1 PR and solvent (water) molecules (system-I), and second the rectangular box includes a fullerene analogue in the binding site of the enzyme and solvent (water) molecules (system-II). Systems I and II are shown in Figure 1. The most potent compound in Table 1 (compound **1**) was docked in the binding cavity of HIV-1 PR and flexible docking has been employed using the FlexX docking program of SYBYL molecular modeling package. The coordinate file of the best FlexX molecular docking pose (which is associated with the biggest (in absolute value) binding energy) is used for system-II.

HIV-1 PR is a  $C_2$  symmetric homodimer with a large substrate binding pocket covered by two glycine-rich  $\beta$ -hairpins, or flaps.<sup>17</sup> Consistent structural differences have been found between the free and bound systems of the HIV-1 PR (average structures from simulation have been considered; in Figure 2, initial forms have been shown with turquoise color and average structures from simulation have been shown with red color). In the fullerene inhibitor-bound forms, the flaps are pulled in toward the dual Asp25 catalytic site (the closed form), while the structure for the free HIV-1 PR adopts a semi-open form with flaps shifted away from the catalytic site, however, still substantially closed to the active site. The

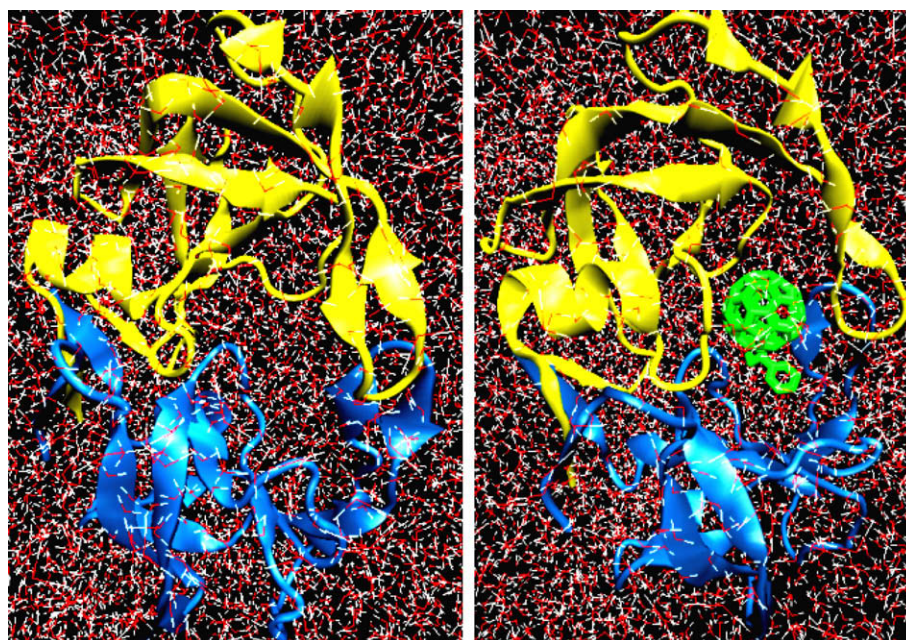


**Figure 1.** Two different systems are used in MD simulations: (i) A ligand-free rectangular box with HIV-1 PR and solvent (water) molecules (system-I) (left on the figure), and (ii) the rectangular box includes fullerene analogue at the binding site of the enzyme and solvent (water) molecules (system-II) (right on the figure).

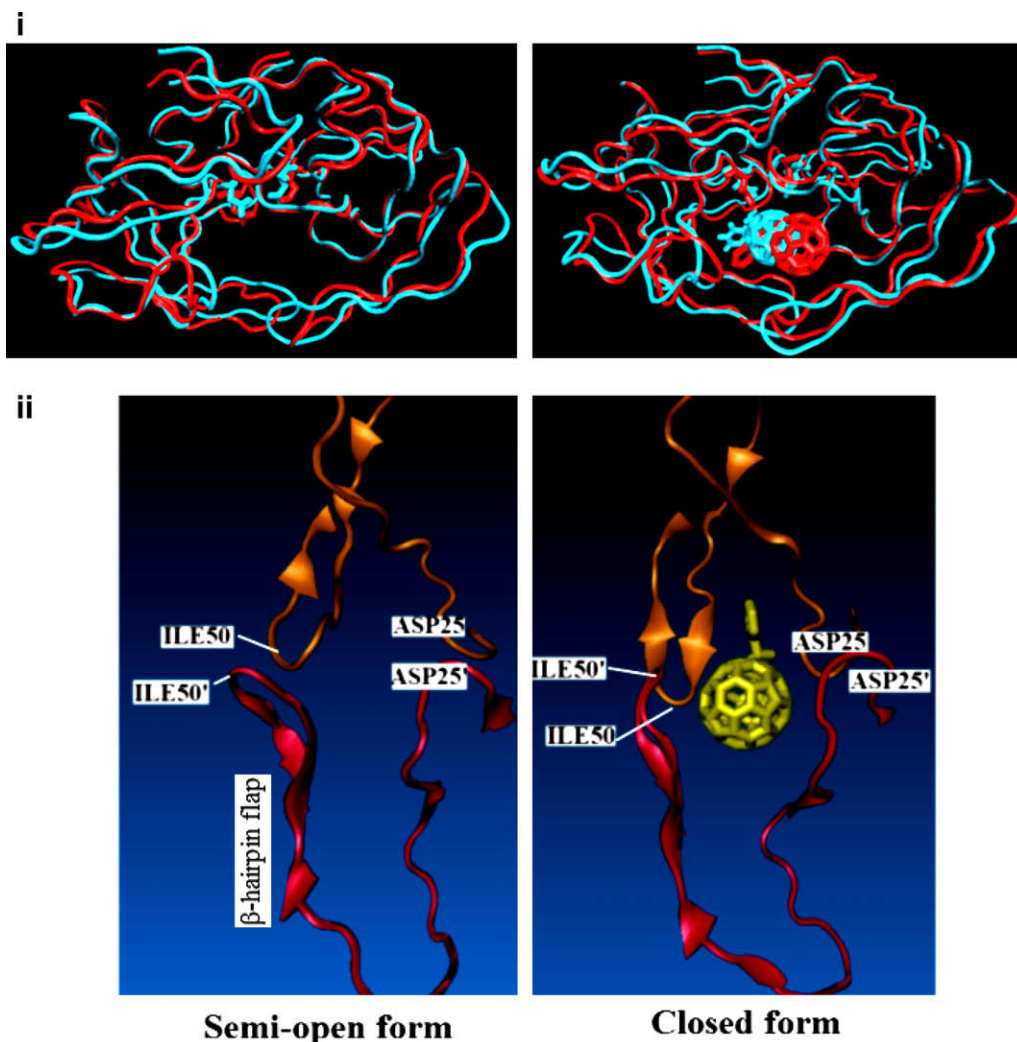


**Figure 2.** (i) In the fullerene inhibitor-bound forms, the flaps are pulled in toward the bottom of active site (the closed form), while the structure for the free HIV-1 PR adopts a semi-open conformation with flaps shifted away from the dual Asp25 catalytic site, however still substantially close to the active site. In figure, initial forms are shown with turquoise color and average structures of simulation are shown with red colors. For clarity, only heavy atoms of the fullerene have been shown in the average structure of the simulation; (ii) A side-view of binding cavity of HIV-1 PR (from average structures of MD simulations of free (left) and inhibitor bound (right) systems) illustrates the semi-open and closed forms.

relative orientation of the  $\beta$ -hairpin flaps is reversed in the two forms (Fig. 2). The results are in agreement with the MD simulations of non-fullerene based HIV-1 PR inhibitor.<sup>17</sup>

Changes of the HIV-1 PR binding cavity for the free and fullerene-bound systems were evaluated by employing the change of distance between  $C^\alpha$  atoms of the two catalytic residues, Asp25 and Asp25', as well as, the change of distance between  $C^\alpha$  atoms of the residues at the flap region (Gly48, Gly49, Ile50, Gly51 and Gly52 amino acid residues in chain A and their corresponding residues in chain B). In the ligand-free system, only some perturbations around the initial distance have been found for the distance between  $C^\alpha$  atoms of Asp25 and Asp25'; Gly48 and Gly48'; Gly51 and Gly51'; Asp25' and Gly49'; Gly52 and Gly52', however, distances between the  $C^\alpha$  atoms have been found increased  $\sim 4$  Å between Asp25 and Gly49;  $\sim 1$  Å between Gly49 and Gly49'; and  $\sim 0.5$  Å between Ile50 and Ile50' through the simulations (Fig. 3i). In the fullerene-bound system a detectable decrease in distances has been observed during the simulation with some perturbations at certain intervals (Fig. 3ii). For example, distances between  $C^\alpha$  atoms have been decreased  $\sim 1.5$  Å between Asp25 and Asp25';  $\sim 0.5$  Å between Gly49 and Gly49';  $\sim 2.0$  Å between Asp25' and

Gly49';  $\sim 2.0$  Å between Gly48 and Gly48'. Distances between Ile50 and Ile50'; Gly51 and Gly51'; Gly52 and Gly52' did not change significantly throughout the simulations (Fig. 3ii). A small increase in the distance ( $\sim 1.0$  Å) has been observed between the  $C^\alpha$  atoms of the amino acids Asp25 and Gly49. Therefore, fullerene inhibitor tends to keep HIV-1 PR cavity in a closed form.

The difference of behavior at the flap region for these systems leads to two different orientations. It has been observed that flap loop of chain A lies perpendicular to that of chain B in both the fullerene bound and ligand free systems. However, in contrast to the ligand free system, chains orient toward the catalytic dual Asp25 residues in fullerene bound system.

The torsional angles ( $OD2-C^\gamma-C^\beta-C^\alpha$ ) of the catalytic dyad (Fig. 4i) were also investigated for the ligand-free and ligand-bound systems. The trajectory analysis of the defined torsional angles of Asp25 and Asp25' for ligand free HIV-1 PR have shown that they keep their value mainly at  $\sim 140^\circ/\sim 300^\circ$  and  $\sim 100^\circ/\sim 300^\circ$ , respectively (Fig. 4ii). These values are  $\sim 200^\circ$  for Asp25 and  $\sim 280^\circ$  for Asp25' in fullerene-bound HIV-1 PR (Fig. 4iii).

Atom positions between the crystal (1AID) and the average structure from MD have been compared for both systems I and II

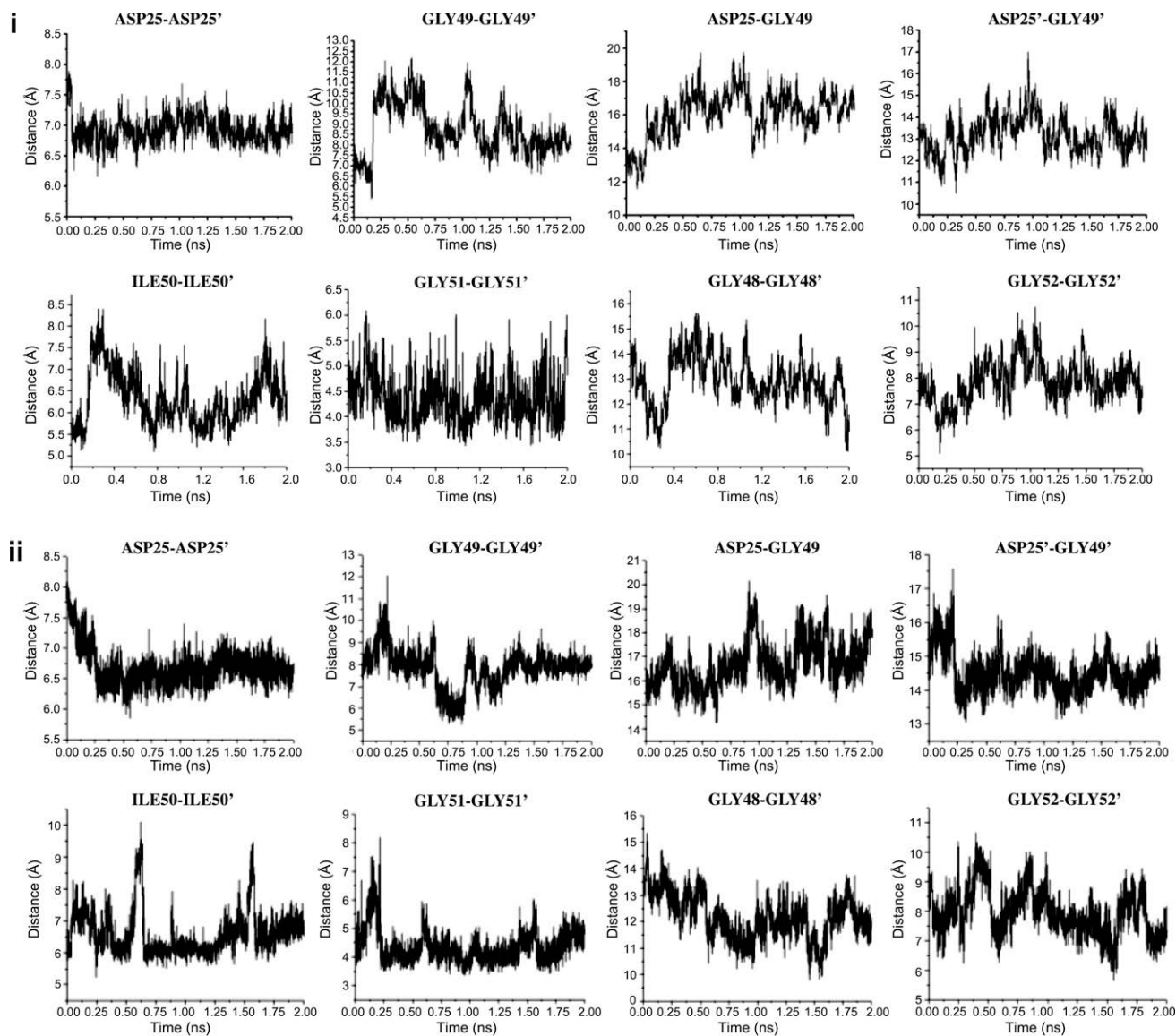


**Figure 3.** (i) Change of the HIV-1 PR binding cavity for the ligand-free (system-I) (ii) and fullerene-bound (system-II) systems were evaluated in terms of distance between the catalytic residues, Asp25 and Asp25' as well as distance between the residues of the flap region (Gly48, Gly49, Ile50, Gly51 and Gly52).

in order to understand which parts of the receptor are more stable and which are floppy. For this purpose, a script with color scale has been used under VMD program (version 1.8.6)<sup>41</sup> where blue colored places show no change in distance (stable) and red colored places show floppy areas (Fig. 5). As it is clearly shown, flap regions, catalytic part, and termino-lateral fields of HIV-1 PR at both systems I and II show more flexible conformations throughout the simulations.

After obtaining the average structure of HIV-1 PR from MD simulations, computed binding energies of the synthesized fullerene analogues (Table 1) from docking simulations were compared with their corresponding experimental results (Table 1). The linearity of the plot ( $r^2 = 0.69$ ,  $N = 19$ , compound **20** is used as outlier) shows a good correlation between computed and experimental binding energies, (Fig. 6).

A designed series of [60]fullerene derivatives based on SAR studies and of biologically evaluated compounds have been subjected to flexible docking using FlexX docking algorithm. The bisadducts of [60]fullerene have a *trans-1* ( $D_{2h}$ ) addition pattern (the nomenclature of the bisadducts followed Hirsch suggestions,

who considers the relative position between addends).<sup>42</sup> A molecular docking algorithm is used for the prediction of potential binding modes of all fullerene derivatives in the binding site of the HIV-1 PR. Since ionization states of these derivatives have not yet been determined experimentally, throughout the docking simulations both neutral and ionized forms are considered. Tables 1 and 2 show the list of fullerene derivatives used in molecular docking studies, their binding energies and their estimated binding affinities from computed binding energies.

In order to design novel fullerene derivatives with high inhibition effect of HIV-1 PR, 3D QSAR/CoMSIA models were employed. As it is mentioned above, binding affinity results from experimental measurements of fullerene-based inhibitors at the HIV-1 PR are limited. Since experimental and computed binding energies showed a good correlation, both experimental binding affinities of structures at Table 1 and estimated binding affinities of structures at Table 2 have been used to form 3D QSAR models. The used structures have a wide variation of biological activity ( $\sim 10^6$ -fold variances in binding affinity). Forty-three molecules in Tables 1 and 2 were used as the training set and the rest 6 derivatives (com-

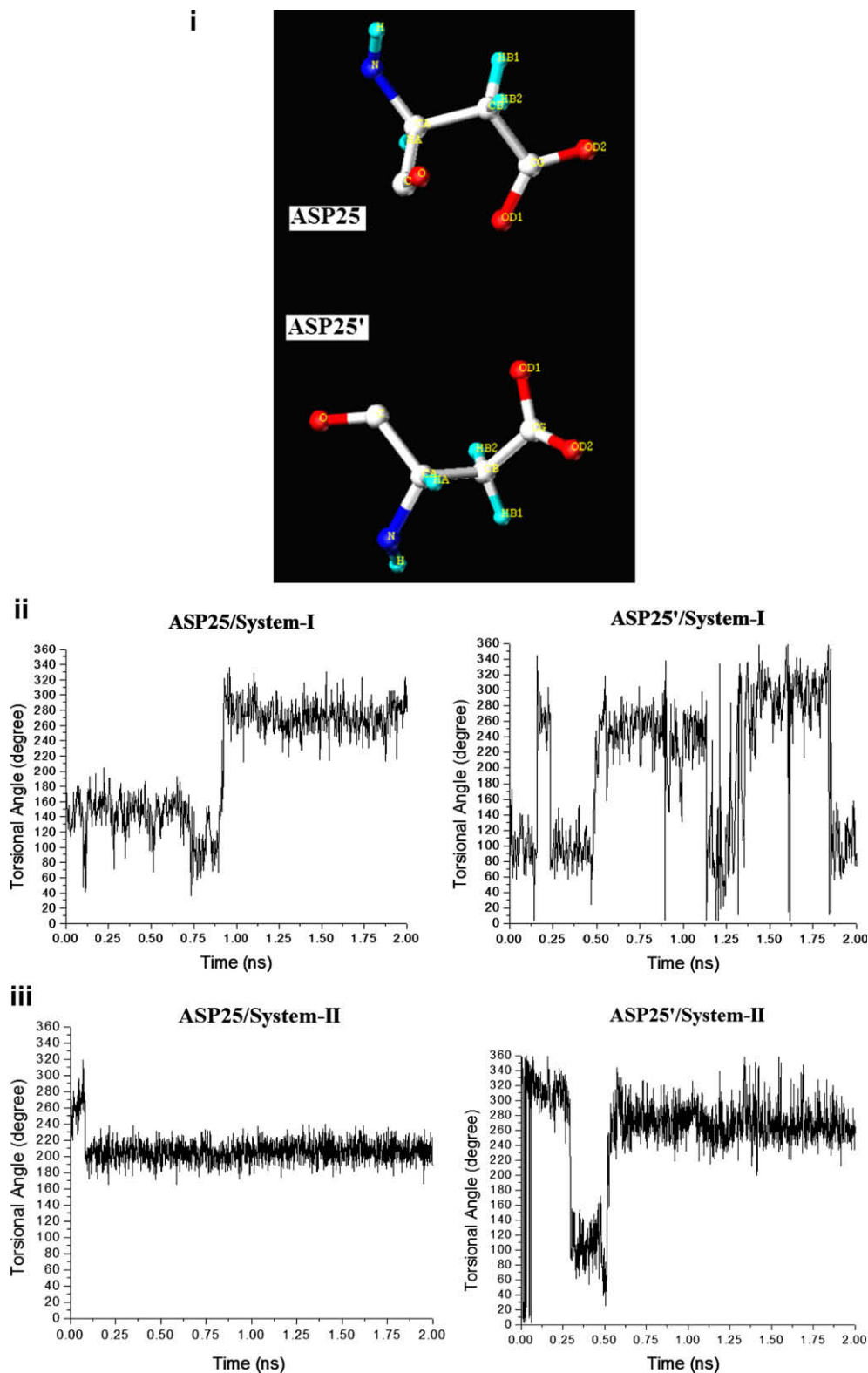


**Figure 4.** (i) The torsional angle of (OD2-C $\gamma$ -C $\beta$ -C $\alpha$ ) of the catalytic dyad for the (ii) ligand-free and the (iii) ligand-bound systems throughout the MD simulation.

pound numbers: **16**, **27**, **34**, **39**, **43** and **48**) were used as test set at the CoMSIA analysis. The test set includes compounds representing all categories of activity of the training set, that is, inactive and active compounds comprising all structural features that are important for the activity. Among the synthesized analogues, compound

**23** was selected as a template, because it has the highest binding affinity at the HIV-1 PR in the training set. Several variations in the alignment schemes are considered by superimposing the similar pharmacophoric features. Highlighted carbon atoms (32 central carbon atoms of fullerene) for the template ligand **23** are

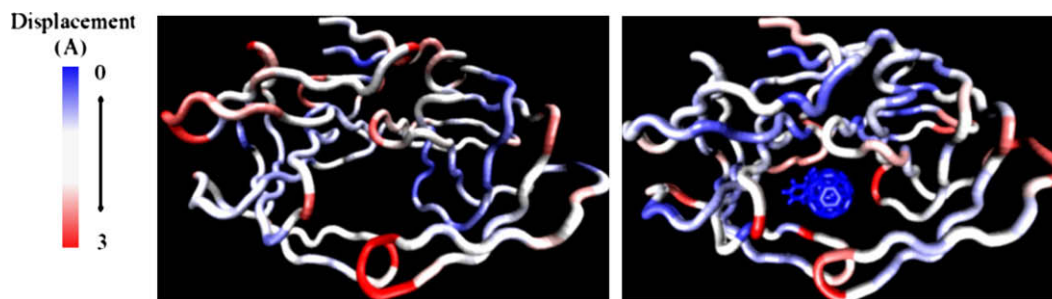


**Figure 5.** Atom positions between the crystal (1AID) and the average structure from MD simulations have been compared for both systems I and II in order to understand which parts of the enzyme are more stable and which are floppy. Blue colored fields show no change in displacement, red colored fields show high flexible regions.

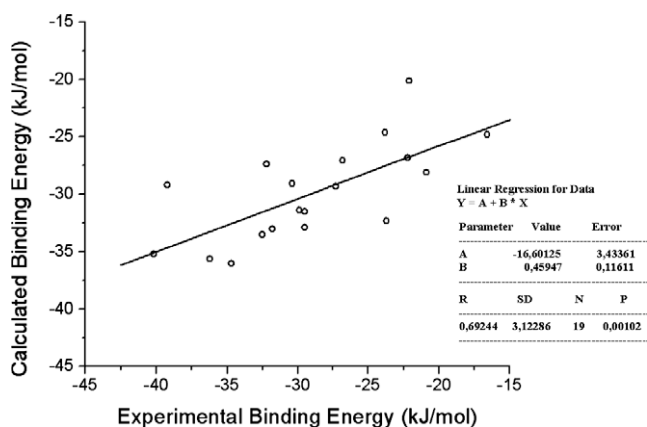


**Figure 6.** Plot of experimental and computed binding energies for the reported fullerene analogues.

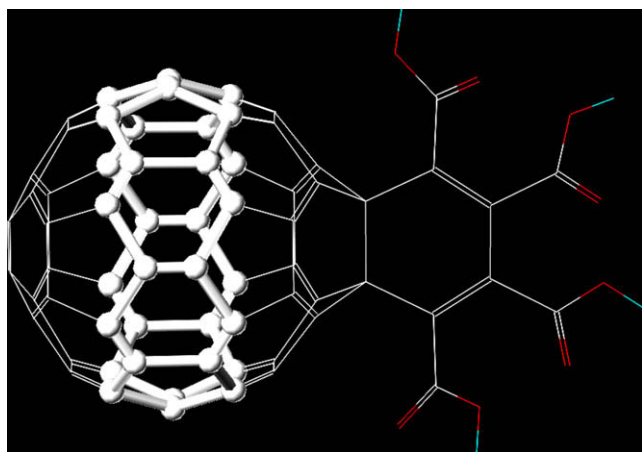


**Figure 7.** Selected atoms of the template compound **23** for structural superimpositions of the compounds in training set.

selected for the structural superimposition processes (Fig. 7). The alignment of the molecules was based on atom-by-atom superimposition of selected atoms, which are common in all compounds. The criteria applied for the selection were: (i) the overlap of the putative biologically relevant pharmacophore groups (with minimum RMSD); (ii) the use of the conformations of subgroups of fullerene derivatives obtained from the docking simulations and (iii) the statistical significance of the 3D-QSAR/CoMSIA models. Figure 8 illustrates the superimposition of fullerene analogues used as the training set to construct CoMSIA models. The cross validated

PLS method was then applied to the training set. Table 3 summarizes the statistical results.

Five different combinations of stereoelectronic fields of 3D QSAR/CoMSIA models were obtained from the set of biologically evaluated and computationally designed fullerene derivatives (training set = 43, test set = 6) in order to predict novel compounds with improved inhibition effect. The best 3D QSAR/CoMSIA model (CoMSIA-4: steric/electrostatic/H-bond donor/H-bond acceptor) yielded a cross validated  $r^2$  value of 0.739 and a non-cross validated  $r^2$  value of 0.993. Using the neutral and ionized states of the fullerene analogues in data set did not affect significantly the constructed QSAR models. Thus, neutral states of fullerene derivatives were used in the further analyses. The selected 3D-QSAR/CoMSIA model (CoMSIA-4) for the estimated binding affinities of fullerene analogues at the HIV-1 PR has a good cross validated correlation. Figure 9 shows the relationship between the estimated  $pEC_{50}$  values from FlexX binding energies and CoMSIA-predicted results of the non-cross-validated analyses for the HIV-1 PR. Linearity of the plot shows very good correlation for the CoMSIA model. Table 4 summarizes the estimated binding affinities from molecular docking results and CoMSIA-predicted  $pEC_{50}$  results for the fullerene derivatives at the HIV-1 PR. A good correlation was observed in CoMSIA of the fullerene derivatives as it is demonstrated by the very high values of  $r^2$ . Additionally, the credibility of the models is evidenced by the high values of  $r_{cv}^2$ . However, the real significance of the proposed model is verified by the good predictions of the activity of compounds belonging to the test set (Table 5). Their  $pEC_{50}$  values of these compounds ranges between 4.04 and 6.74 and their biological activities were predicted from the PLS equations derived from CoMSIA-4 model. All compounds showed predicted values within one logarithmic unit difference from the estimated  $pEC_{50}$  values.

The contour maps are used to create a matrix in the place of the active site and variations of the used ligands can be generated as long as they fit better into the binding site. Figure 10i shows the steric-electrostatic contour maps of the CoMSIA models for the compounds **23** that shows the highest and **36** that shows the lowest inhibition effects within the data set for the HIV-1 PR enzyme (see Tables 1 and 2). The individual contributions from the steric and electrostatic favored and disfavored levels are fixed at 80% and 20%, respectively. The contours for steric fields are shown in green (bulky groups favored) and yellow (bulky groups not favored) while the electrostatic field contours are shown in red (electronegative substituents favored) and blue (electropositive substituents favored). In addition, H-bond donor and H-bond acceptor contour maps have been shown in Figure 10ii. The individual contributions from the H-bond donor and H-bond acceptor favored and disfavored levels are fixed at 80% and 20%, respectively. The contours for H-bond donor favored fields have been shown in cyan color while its disfavored fields have been shown in purple color. H-bond acceptor favored fields have been shown

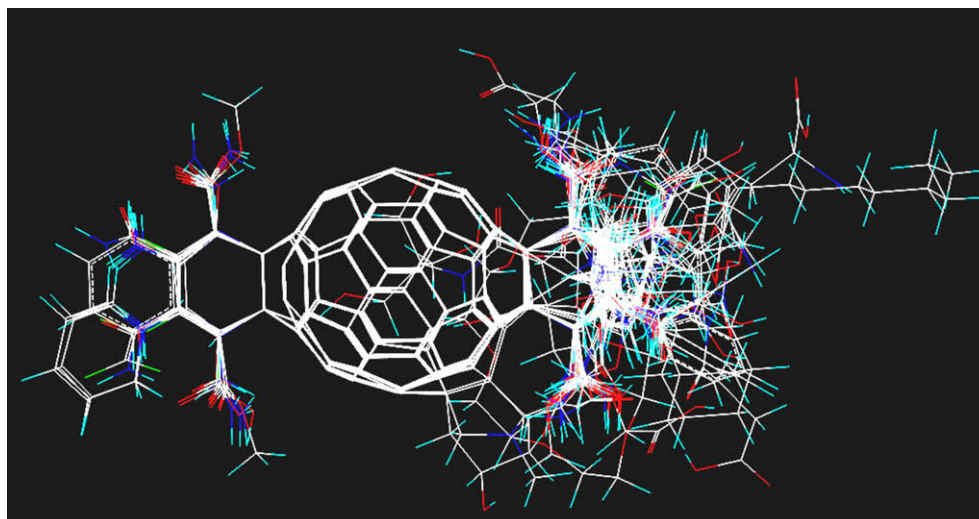


Figure 8. Structural alignment of the compounds in the training set for constructing 3D-QSAR/CoMSIA model at HIV-1 PR.

Table 3

Summary of statistical results of the derived CoMSIA models for the training set.

	CoMSIA1 (STR/ES)	CoMSIA2 (STR/ES/ACC)	CoMSIA3 (STR/ES/DON)	CoMSIA4 (STR/ES/ACC/DON)	CoMSIA5 (STR/ES/ACC/DON/HYD)
$r_{cv}^2$	0.616	0.733	0.630	0.739	0.670
$r^2$	0.970	0.991	0.985	0.993	0.993
Components	6	6	6	6	6
$F$	191.713	632.364	392.176	824.144	861.108
Std. Err.	0.266	0.148	0.188	0.130	0.127
Rel. Contr. Steric	0.707	0.512	0.551	0.426	0.243
Electrostatic	0.293	0.143	0.197	0.127	0.086
Hydrophobic	–	–	0.252	–	0.369
H-bond donor	–	–	–	0.167	0.109
H-bond acceptor	–	0.345	–	0.280	0.193

Abbreviations: STR, steric; ES, electrostatic; ACC, H-bond acceptor; DON, H-bond donor; HYD, hydrophobic.

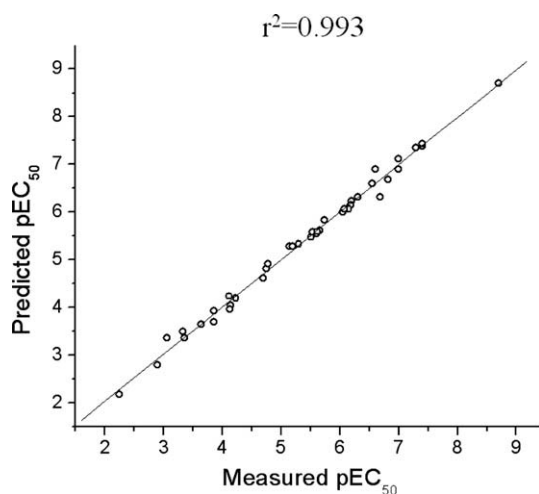


Figure 9. Plot of measured and CoMSIA-predicted binding affinities (given as  $pEC_{50}$ ) of fullerene analogues in the training set at the HIV-1 PR.

in orange color while its disfavored fields have been shown in white color.

Derived 3D contour maps of CoMSIA models are investigated in the binding cavity of the HIV-1 PR. Contour plots confirmed the stability of the constructed models. For example, the estimated

$EC_{50}$  values of **23** and **36** are in nM and in mM ranges, respectively. This can be explained by different topographical requirements for **23** and **36**, in contour maps (Fig. 10). There are large yellow colored contours close to the flap regions of HIV-1 PR. Compound **36** shows the existence of sterically unfavorable fields (the areas in which bulky groups are predicted to decrease binding). A part of cyclohexadiene and dihydropyridine groups of **36** fits with these unfavorable regions; right in Fig. 10i). However, sterically unfavorable yellow colored contour maps do not match with the subgroups of **23** (left in Fig. 10i). Furthermore, the subgroups of **23** fit perfectly with the sterically favorable areas which are shown with green colored contours (left in Fig. 10i). Electrostatic contour maps (shown with blue and red colored contour maps) are mainly observed in the catalytic region of binding cavity. Red colored contours which show electronegative favored fields are in very close neighborhood with the  $-COOH$  groups of **23**. H-bond donor and H-bond acceptor contour maps have been shown in Figure 10ii in the binding cavity of HIV-1 PR. H-bond acceptor and H-bond donor favored regions fit very well with the  $-COOH$  groups of **23** and disfavored regions are far from the subgroups of the **23** (left in Fig. 10ii). However, subgroups of **36** fit mainly with the purple colored contours which are disfavored for the H-bond donor interactions (right in Fig. 10ii).

Leapfrog de novo drug design software has been used to propose novel fullerene HIV-1 PR inhibitors. Molecules **1**, **3** (biologically measured potent molecules, Table 1), **23** and **42** (computationally designed monoadduct and bisadduct fullerene

**Table 4**  
Measured and 3D QSAR/CoMSIA predicted binding affinities of compounds in training set.

Compound No.	Measured pEC <sub>50</sub>	3D QSAR CoMSIA Predicted pEC <sub>50</sub>	Difference
1	7.0	6.90	0.10
2	5.3	5.33	-0.03
3	6.82	6.69	0.13
4	5.14	5.28	-0.14
5	6.31	6.32	-0.01
6	2.89	2.80	0.09
7	4.12	4.24	-0.12
8	3.64	3.65	-0.01
9	3.85	3.70	0.15
10	5.60	5.55	0.05
11	6.05	5.99	0.06
12	5.14	5.28	-0.14
13	5.66	5.62	0.04
14	5.20	5.28	-0.08
15	5.54	5.58	-0.04
17	3.86	3.93	-0.07
18	4.75	4.81	-0.06
19	4.14	4.05	0.09
21	6.60	6.90	-0.30
22	7.29	7.34	-0.05
23	8.70	8.70	0.00
24	6.15	6.07	0.08
25	3.33	3.49	-0.16
26	6.20	6.24	-0.04
28	6.18	6.15	0.03
29	6.68	6.31	0.37
30	4.70	4.62	0.12
31	4.77	4.92	-0.15
32	5.50	5.47	0.03
33	6.55	6.59	-0.04
35	4.23	4.19	0.04
36	2.25	2.18	0.07
37	3.36	3.36	0.00
38	5.73	5.83	-0.10
40	3.06	3.36	-0.30
41	7.40	7.38	0.02
42	7.40	7.43	-0.03
44	5.61	5.59	0.02
45	4.13	3.96	0.17
46	7.00	7.12	-0.12
47	6.15	6.07	0.08
49	6.08	6.07	0.01

**Table 5**  
Measured and 3D QSAR/CoMSIA predicted binding affinities of compounds in test set.

Compound	Measured pEC <sub>50</sub>	3D QSAR CoMSIA Predicted pEC <sub>50</sub>	Difference
16	4.66	5.39	-0.73
27	5.82	5.31	0.51
34	4.04	3.67	0.37
39	4.61	5.60	-0.99
43	6.74	7.68	-0.94
48	5.22	5.47	-0.25

derivatives that have best predicted binding energy with HIV-1 PR, Table 2) were used as starting structures with allowing the modifications only for the subgroups of fullerene derivatives in Leapfrog simulations. In addition to the de novo drug design, 3D QSAR/CoMSIA contour maps were also used to design new monoadducts and bisadducts [60]fullerene. More than 100 compounds have been designed to vary in polarity and contain various groups exerting electrostatic and steric interactions at different topographical requirements and their binding energies with HIV-1 PR have been computed using molecular docking studies (structures and computed binding energies of these fullerene derivatives are presented in supporting information, Table S1). These are expected to differ in their mode of action as it is indeed observed with the active site of

the receptor. The binding interactions of **1** (high potent biologically evaluated fullerene derivative, Table 1) and **23** (computationally designed fullerene derivative with predicted very high potency, Table 2) at the active site of the HIV-1 PR have been compared in Figure 11. Compound **1** forms two hydrogen bonds between hydrogen atom of -OH group of ligand and oxygen atoms of the -COO group of Asp25 catalytic amino acid residue at chain B, together with oxygen atom of -OH group of ligand and hydrogen atom of backbone -NH group of Ala28 at chain B (left in Fig. 11). On the other hand, **23** forms a hydrogen bond network between -COOH groups of ligand and catalytic amino acid residues Asp25, Gly27, Asp29, Asp30 at chain A together with Asp25 and Gly27 at chain B (right in Fig. 11). The van der Waals interactions of these ligands with non-polar HIV-1 PR surface have been observed mainly at the flap part of the cavity.

It must be noted that this is a computational study, thus the feasibility of synthesizing any of the designed derivatives has not been thoroughly examined.

#### 4. Conclusions

The aim of this study was to investigate the binding interactions of fullerene inhibitors at the active site of the HIV-1 PR, in order to design novel fullerene compounds with enhanced activity. Although the size of the [60]fullerene may seem large for a drug candidate, it has roughly similar size (~10 Å) with many small pharmaceutical molecules.<sup>5</sup> Perfect fitness of fullerene inhibitor at the active site of the HIV-1 PR has been depicted in Fig. S1 of supporting information. The binding interactions of [60]fullerene derivatives at the cavity of the HIV-1 PR have been examined using a combination of molecular docking, 3D QSAR and MD simulations studies.

MD simulations were applied to the ligand-free and ligand-bound HIV-1 PR. MD simulations assisted to have correct enzyme input coordinates for the docking studies as well as contributed substantially in the understanding of the structural changes at the catalytic and flap regions for these two different systems. Structural differences have been found between the unbound and bound systems of the binding cavity of HIV-1 PR. In the fullerene inhibitor-bound forms, the flaps are pulled in toward the bottom of active site (the closed form), while, the structure for the free HIV-1 PR adopts a semi-open conformation with flaps shifted away from the dual Asp25 catalytic site. Both MD simulations have shown that flap, catalytic and termino-lateral regions of HIV-1 PR show more flexibility during the simulations.

A series of fullerene derivatives have been designed and their binding energies with HIV-1 PR have been computed with molecular docking analysis. The correlation between structures and binding affinities has been studied with CoMSIA method of 3D QSAR. High relative contributions of steric fields from derived contour maps of CoMSIA models confirm the importance of the van der Waals interactions with non-polar HIV-1 PR surface in the activity of fullerenes. The contour maps from constructed 3D QSAR/CoMSIA models together with Leapfrog de novo drug design studies assisted to propose novel fullerene derivatives with better predicted potency.

In conclusion, in this study the topological requirements of the fullerene derivatives were revealed by employing a 3D QSAR model. The connection between the biological activity and the conformational changes occurring at the catalytic site of the HIV-1 PR, have been discussed using docking and dynamics simulations. This information is useful to rationalize the molecular basis of fullerene HIV-1 PR inhibition. This study can aid synthetic chemists to initiate the synthesis of novel fullerene derivatives as HIV-1 PR inhibitors.



8. Friedman, H. S.; Ganapathi, P. S.; Rubin, P. S.; Kenyon, G. L. *J. Med. Chem.* **1998**, *41*, 2424.
9. Durdagi, S.; Mavromoustakos, T.; Papadopoulos, M. G. *Bioorg. Med. Chem. Lett.* in press.
10. Bingel, C. *Chem. Ber.* **1993**, *126*, 1957.
11. Ganapathi, P. S.; Friedman, S. H.; Kenyon, G. L.; Rubin, Y. *J. Org. Chem.* **1995**, *60*, 2954.
12. Schuster, D. I.; Wilson, S. R.; Schinazi, R. F. *Bioorg. Med. Chem. Lett.* **1996**, *6*, 1253.
13. Available from: <http://www.chemdb.niaid.nih.gov>.
14. An, Y.-Z.; Ellis, G. A.; Viado, A. L.; Rubin, Y. *J. Org. Chem.* **1995**, *60*, 6353.
15. Klebe, G.; Abraham, U.; Mietzner, T. *J. Med. Chem.* **1994**, *37*, 4130.
16. Hornak, V.; Okur, A.; Rizzo, R. C.; Simmerling, C. *Proc. Nat. Am. Sci.* **2006**, *103*, 915.
17. Hornak, V.; Okur, A.; Rizzo, R. C.; Simmerling, C. *J. Am. Chem. Soc.* **2006**, *128*, 2812.
18. Zhu, Z.; Schuster, D. I.; Tuckerman, M. E. *Biochemistry* **2003**, *42*, 1326.
19. Sybyl molecular modeling software packages, ver. 6.8., 2001, Tripos Inc., St. Louis, MO 63144.
20. Powell, M. J. D. *Math. Prog.* **1977**, *12*, 241.
21. Gasteiger, J.; Marsili, M. *Tetrahedron* **1980**, *36*, 3219.
22. Rutenber, E.; Fauman, E. B.; Keenan, R. J.; Fong, S.; Furth, P. S.; Ortiz de Montellano, P. R.; Meng, E.; Kuntz, I. D.; DeCamp, D. L.; Salto, R.; Ros, J. R.; Craik, C. S.; Stroud, R. M. *J. Biol. Chem.* **1993**, *268*, 15343.
23. Frimurer, T. M.; Peters, G. H.; Iversen, L. F.; Andersen, H. S.; Moller, N. P. H.; Olsen, O. H. *Biophys. J.* **2003**, *84*, 2273.
24. Soares, T. A.; Goodsell, D. S.; Ferreira, R.; Olson, A. J.; Briggs, J. M. *J. Mol. Recognit.* **2000**, *13*, 146.
25. Locuson, C. W.; Gannett, P. M.; Ayscue, R.; Tracy, T. S. *J. Med. Chem.* **2007**, *50*, 1158.
26. AbuHammad, A. M.; Affif, F. U.; Taha, O. M. *J. Mol. Graph. Model.* **2007**, *26*, 443.
27. Koehler, K. F.; Rao, S. N.; Snyder, J. P. *Guidebook on Molecular Modeling in Drug Design*; Academic Press: San Diego, 1996.
28. Böhm, H.-J. *J. Comput.-Aided. Mol. Des.* **1994**, *10*, 427.
29. Van Der Spoel, D.; Lindahl, E.; Hess, B.; Groenhof, G.; Mark, A. E.; Berendsen, H. J. *J. Comput. Chem.* **2005**, *26*, 1701.
30. Lindhal, E.; Hess, B.; van der Spoel, D. *J. Mol. Model.* **2001**, *7*, 306.
31. Berendsen, H. J. C.; Postma, J. P. M.; van Gunsteren, W. F.; Dinola, A.; Haak, J. R. *J. Comput. Chem.* **1984**, *81*, 3684.
32. Essmann, U.; Perera, L.; Berkowitz, M. L.; Darden, T.; Lee, H.; Pedersen, L. G. *J. Chem. Phys.* **1995**, *103*, 8577.
33. Sengupta, D.; Verma, D.; Naik, P. K. *J. Biosci.* **2007**, *32*, 1316.
34. Conn, P. J.; Sanders-Bush, E.; Hoffman, B. J.; Hartig, P. R. *Proc. Nat. Am. Sci.* **1986**, *83*, 4086.
35. Cramer, R. D. I.; Depriest, S.; Patterson, D.; Hecht, P. The developing practice of comparative molecular field analysis; Kubinyi, H., Ed.; ESCOM: Leiden 1993, 443.
36. Durdagi, S.; Kapou, A.; Kourouli, T.; Andreou, T.; Nikas, S. P.; Nahmias, V. R.; Papahatjis, D. P.; Papadopoulos, M. G.; Mavromoustakos, T. *J. Med. Chem.* **2007**, *50*, 2875.
37. Leach, A. R.; Gillet, V. J. *An Introduction to Chemoinformatics*; Kluwer Academic Publishers: Dordrecht, 2003.
38. Nair, C. P.; Sobiha, M. E. *J. Mol. Graph. Model.* **2007**, *26*, 117.
39. Makhija, M. T.; Kasliwal, R. T.; Kulkarni, V. M.; Neamati, N. *Bioorg. Med. Chem.* **2004**, *12*, 2317.
40. Kapou, A.; Benetis, N. P.; Durdagi, S.; Nikolaropoulos, S.; Mavromoustakos, T. *J. Chem. Info. Model.* in press.
41. Humphrey, W.; Dalke, A.; Schulten, K. *J. Mol. Graph.* **1996**, *14*, 33.
42. Hirsch, A.; Lamparth, I.; Karfunkel, H. R. *Angew. Chem. Int. Ed. Engl.* **1994**, *33*, 437.